

3D PRINTED DIFFRACTIVE LENSES OPERATING AT 1 THz

P. Komorowski ^a, M. Kaluza ^b, M. Surma ^b, and A. Siemion ^b

^a *Institute of Optoelectronics, Military University of Technology, 00908 Warsaw, Poland*

^b *Faculty of Physics, Warsaw University of Technology, 00662 Warsaw, Poland*

Email: pawel.komorowski@wat.edu.pl

Received 17 September 2023; accepted 18 September 2023

In this paper, we demonstrate the manufacturing of diffractive optics for frequencies as high as 1 THz using a relatively simple and cost-effective fused deposition modelling (FDM) 3D printing technique. Four diffractive lenses were designed and manufactured from the cyclic olefin copolymer (COC). Fabrication of diffractive lenses for such high frequencies was possible due to an unusually small nozzle, refined printing procedures and a very transparent material. For the two of the manufactured lenses, more than twofold improvement in focusing efficiency has been shown in a direct comparison with their refractive counterparts. Moreover, the other two elements demonstrated the feasibility of lenses with very small f -numbers (0.95 and 0.63) with this technique.

Keywords: THz, 3D printing, optics, lenses, diffractive optical elements

1. Introduction

The study on terahertz (THz) radiation remains a fast-developing field in the last decades [1]. The remarkable progress in the construction of efficient emitters [2] and detectors [3] of THz radiation leads the way toward more and more new applications of THz waves. They have already been implemented in telecommunication systems [4–6], medical diagnostics [7–9], material studies [10–12] and security systems [13–15], to name only a few.

Various THz radiation applications encourage the development of all kinds of optics dedicated to this spectral range. The reflective, refractive, or diffractive approach might be taken depending on the particular usage. Reflective optics (different types of mirrors) offer low-loss and broad-band operation, at the cost of bulkiness, higher manufacturing cost, and complexity of the optical setups. The transmissive optics (refractive and diffractive), on the other hand, suffer from chromatic aberration and strongly depend on the optical parameters of the materials used in the manufactur-

ing process of optical elements. However, they are more compact, lightweight, and usually simpler to fabricate. The effect of chromatic aberrations is more significant in diffractive optics, where the structure shape is precisely determined in relation to the wavelength of radiation. Therefore, the physics of diffraction limits the spectral operational band of such elements, while in the case of refractive optics the limitation is much less significant and comes only from the dispersion of the material. It must be noted, though, that diffractive optical elements (DOEs) also have important and distinctive advantages. First, the phase maps describing the DOEs can be calculated to reshape the incoming radiation into practically arbitrary intensity profiles. Moreover, the thickness of DOEs is usually in the order of the wavelength, which makes them exceptionally thin and subsequently much more transparent than their refractive counterparts.

For frequencies in the range 0.1–0.6 THz, DOEs can be manufactured relatively easily and inexpensively from polymers using additive manufacturing technologies [16–18]. However,

manufacturing with this method becomes tricky for higher frequencies. It is connected with two facts – the wavelength dependence of the size of DOEs details and the absorption coefficient of the available materials. The first issue can be partially solved using higher-order kinoforms [19]. Although effective, this approach limits the design space of DOEs. Higher-order kinoforms are thicker, resulting in a higher attenuation of an element. Therefore, seeking methods of manufacturing first-order kinoforms is still desirable.

Thanks to the advancement of 3D printing technologies, new possibilities of printing with a high resolution became achievable. Taking into account the fused deposition modelling (FDM) technique, small nozzles are being utilized for the manufacturing of three-dimensional objects, which currently achieve diameters as small as $150\ \mu\text{m}$. This ensures a thin line in the manufacturing process, which accurately captures the intricate details of the 3D spatial model. Moreover, high-quality nozzles are covered with a non-adhesive coating (e.g. tungsten disulfide fullerene structure (WS_2) nanoparticles) guaranteeing the appropriate shape of printing lines. In addition, the nozzles provide a stable temperature and material flow in the printing process. Therefore, clogging of the nozzle, which frequently occurs in the case of small nozzles, can be avoided.

The popularity of FDM 3D printing results in the vast selection of available filaments. Some of them, such as cyclic olefin copolymer (COC), polypropylene (PP), or styrene butadiene copolymer (SBC), are characterized by very good optical properties in the THz spectral range [16, 20]. The mentioned materials exhibit low absorption coefficients even for frequencies as high as 1 THz, which makes them worthy of consideration for manufacturing DOEs. While the technology matures, the quality of the offered filaments improves, ultimately allowing for the manufacturing of DOEs for higher and higher frequencies. Moreover, manufacturing with the FDM technique avoids significant deformations of flat, broad prints of DOEs, which occur in other additive manufacturing techniques like selective laser sintering.

This paper demonstrates the possibility of manufacturing diffractive optics for frequencies as high as 1 THz using a relatively simple and cost-effective FDM 3D printing technology. The selection of the appropriate printing materials, temperature

settings as well as the cooling process are discussed as well. The manufactured lenses performed better than their refractive counterparts in a direct comparison. Moreover, the diffractive lenses that are practically unachievable by the classical refractive approach have been demonstrated.

2. Lenses

Four diffractive lenses are proposed. The geometrical parameters of the two lenses have been customized to match the commercially available refractive lenses. In this way, a direct comparison of their performance can be carried out. Two PTFE lenses from *Thorlabs Inc.* have been used – a 3" lens with a focal length of $f = 115\ \text{mm}$ (part number LAT115) and a 4" lens with a focal length of $f = 151.5\ \text{mm}$ (LAT151). Moreover, two additional lenses with a 3" diameter and focal lengths of $f = 72.2$ and $f = 48.1\ \text{mm}$ have been proposed. These two lenses are characterized by a very small focal length to diameter ratios (f-numbers). This would make them at least impractical, if not practically infeasible, to be realized with a refractive approach. Thus, the two low f-number lenses, on the one hand, demonstrate the advantages of a diffractive approach, and, on the other, allow one to investigate the limits of this manufacturing method.

2.1. Design

The DOEs are described with a two-dimensional distribution of the phase retardation introduced to the radiation. These distributions, known as phase maps, take the values varying from 0 to 2π and typically have discontinuities, where the phase rapidly shifts from the minimal to the maximal value.

Phase maps of the diffractive kinoform lenses have been calculated according to the theoretical lens equation

$$\phi(x, y) = \exp\left(-i \frac{2\pi}{\lambda} \sqrt{x^2 + y^2 + f^2}\right), \quad (1)$$

where ϕ is the phase retardation, x and y are the Cartesian coordinates, λ is the design wavelength, and f is the focal length. Equation (1) describes the general phase front of the focusing lens of a certain focal length f . It does not assume a paraxial approximation, which makes it suitable for designing lenses with a high f-number. The phase maps of the designed elements are presented in Fig. 1.

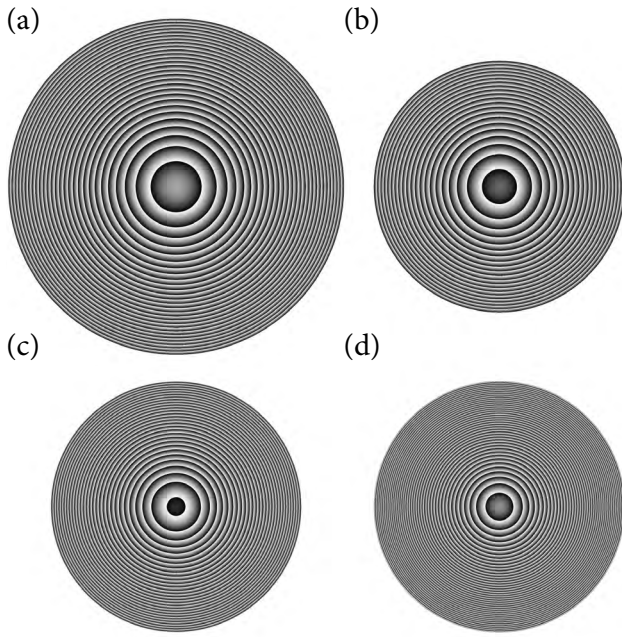


Fig. 1. Phase maps of the designed DOEs: (a) 4'' $f = 151.5$ mm lens, (b) 3'' $f = 115$ mm lens, (c) 3'' $f = 72.2$ mm lens and (d) 3'' $f = 48.1$ mm lens. The black colour represents the relative 0 phase retardation, while the white colour corresponds to the maximal phase delay of 2π .

All lenses have been calculated as bitmaps containing 2048×2048 pixels. In the case of the two lenses with longer focal lengths (Fig. 1(a, b)), the pixel size has been set to $50 \mu\text{m}$, while for the two lenses with shorter focal lengths (Fig. 1(c, d)) this value has been reduced to $40 \mu\text{m}$. The smaller pixel size ensures a more accurate reproduction of the highly-detailed phase maps of high f-number lenses.

2.2. Manufacturing

The phase maps have been transformed into 3D models for additive manufacturing. The height of the structure at any point can be calculated using the formula

$$h(x, y) = \frac{\phi(x, y)}{2\pi} \cdot \frac{\lambda}{n-1}, \quad (2)$$

where h is the relative pixel height, and n is the refractive index of the material used for manufacturing. Equation (2) assumes surrounding of air with the refractive index $n_{\text{air}} \approx 1$.

The maximal height of the designed 3D models is equal to 0.6 mm. Additionally, a substrate with a height of 0.5 mm has been added to the models,

resulting in a total height of 1.1 mm for each DOE. The substrate ensures the stability of the structure and prevents deformation during the manufacturing process.

The diffractive lenses have been manufactured from the COC by means of FDM 3D printing. The optical parameters of COC have been examined using time-domain spectroscopy (THz-TDS). At 1 THz, the absorption coefficient of COC is equal to 0.500 cm^{-1} and the refractive index is equal to 1.512.

The extrusion temperature used in the manufacturing process was equal to 235°C . The temperature is slightly below the manufacturer's recommendation, which helps avoiding nozzle clogging during the printing. During manufacturing, the hardened steel nozzle with electroless nickel plating and WS_2 nanoparticles coating has been used. A nozzle of 0.25 mm size has been used, providing a horizontal printing resolution equal to $250 \mu\text{m}$. The layer thickness of the print has been set to $50 \mu\text{m}$, which corresponds to the vertical resolution of the print. Considering the 0.60 mm thickness of the structures (the substrate is not taken into account), the twelve layers of the print represent the grayscale layers of previously designed bitmaps. The theoretical diffractive efficiency of a multi-level kinoform can be calculated with the formula

$$\eta_m = \frac{\sin^2\left(\frac{m}{N}\right)}{\left(\frac{m}{N}\right)^2}, \quad (3)$$

where m is the order of diffraction, and N is the number of phase levels within the structure. Thus, the 12-level element focuses the radiation into the 1st diffraction order with an efficiency of $\eta_1 = 97.8\%$. Therefore, this approach enables an accurate representation of the 3D model for each diffractive structure. The photographs of the manufactured lenses are shown in Fig. 2.

It should be mentioned that manufacturing of structures for high frequencies such as 1 THz is a challenging task. It requires an extremely precise adjustment of all 3D printing parameters and a proper calibration of the printer as well as multiple attempts at manufacturing. In this case, we are approaching the limit of manufacturing DOEs with FDM technology. The outer zones of low f-number lenses (Fig. 2(c, d)) are so narrow that the details of

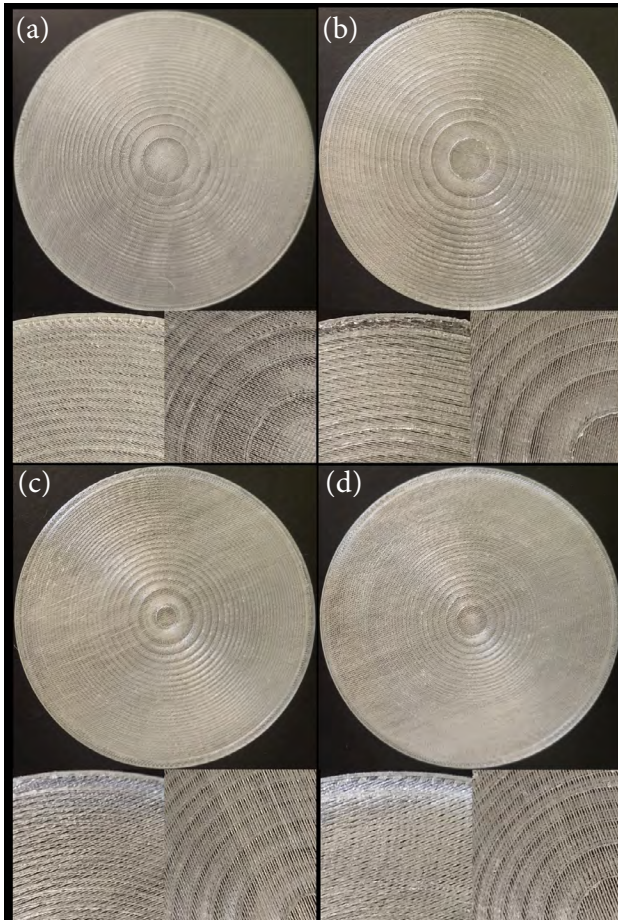


Fig. 2. Photograph of the manufactured lenses: (a) $4''f = 151.5$ mm lens, (b) $3''f = 115$ mm lens, (c) $3''f = 72.2$ mm lens and (d) $3''f = 48.1$ mm lens.

the print are difficult to represent. However, it needs to be highlighted that the application of a smaller nozzle (e.g. with $150\ \mu\text{m}$ diameter) would permit an even higher print resolution. Moreover, smaller nozzles might also be applied for the manufacturing of DOEs for frequencies above 1 THz.

3. Experiment

3.1. Setup

The diagram of the experimental setup is depicted in Fig. 3. A Schottky diode-based frequency multiplier from VDI has been used as a source of radiation. The basic frequency emitted by an yttrium iron garnet (YIG) oscillator has been multiplied 81 times to achieve emission at 1 THz. The emitted divergent wave has been collimated into a quasi-plane wave using an off-axis parabolic mirror. The redirected beam illuminates the evaluated lens, which focuses it on the receiver. The Schottky diode placed in

a waveguide equipped with a horn antenna has been used to detect the radiation. The detector has been placed on a 3D motorized stage, which allows performing raster scanning in a given plane. A Stanford RS830 lock-in amplifier with a 187 Hz modulation has been additionally used to enhance the signal-to-noise ratio in the system. In all cases, the direct value measured is the voltage, which is directly proportional to the incoming optical power.

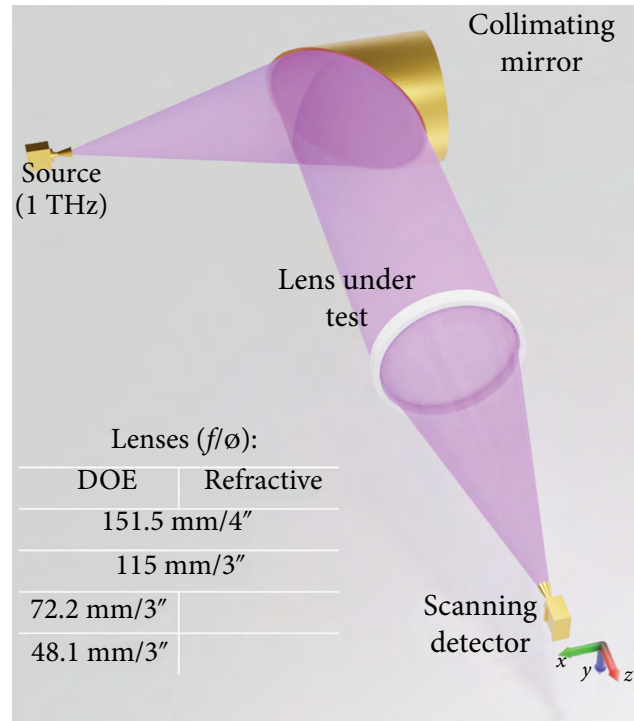


Fig. 3. The diagram of the experimental setup. The radiation diverging from the source is collimated with an off-axis parabolic mirror having a diameter of 8" and forms a quasi-plane wave illuminating the lens under test. Next, at the distance around f after the lens xy and xz plane scans are performed by the scanning detector. The table in the bottom-left summarizes the geometrical parameters of the tested lenses.

Scans in the planes parallel and perpendicular to the main optical axis have been gathered. The vertical plane perpendicular to the optical axis has been denoted as xy , while the horizontal plane containing the optical axis of the system has been named xz (see Fig. 3).

3.2. Results and discussion

The xy scans obtained for two diffractive and two refractive lenses are shown in Fig. 4. The resolution

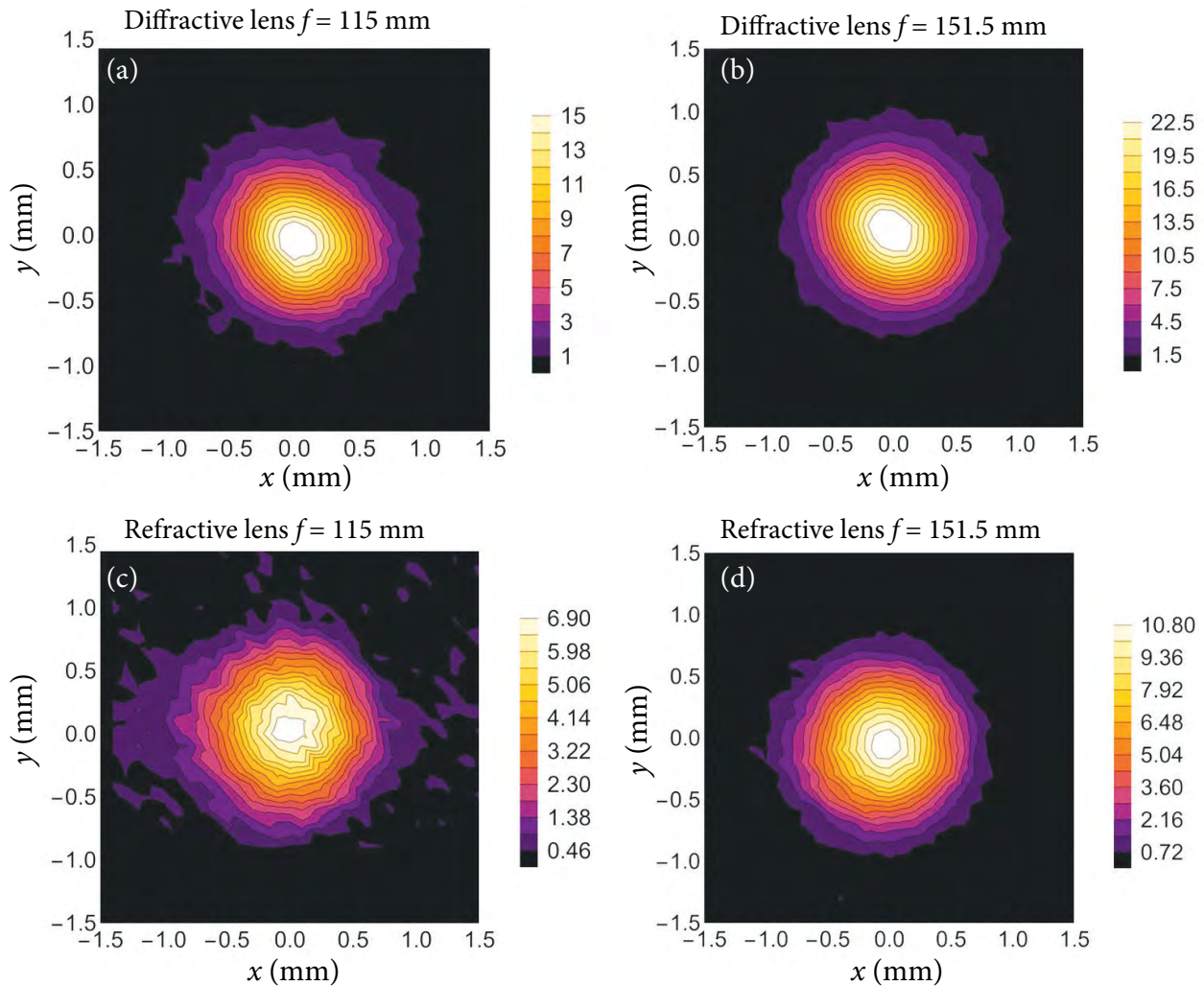


Fig. 4. The perpendicular (xy) scans in focal planes for (a) diffractive lens with $f = 115$ mm, (b) diffractive lens with $f = 151.5$ mm, (c) refractive lens with $f = 115$ mm and (d) refractive lens with $f = 151.5$ mm. The scale is expressed in μW , which is directly proportional to the intensity of radiation.

of scans in both axes is equal to 0.1 mm. In all cases, a well-shaped circular focal spot has been observed. The geometrical parameters of the spots obtained from the designed diffractive and reference refractive lenses are comparable. However, the radiation intensity registered is 2.17 and 2.21 times higher for the $f = 115$ and $f = 151.5$ mm diffractive lenses, respectively.

The longitudinal positions of the focal spots have been verified by performing xz scans. These parallel cross-sections are shown in Fig. 5. The resolution of scans has been set to 0.5 mm in the x axis and to 2 mm in the z axis. The distance z is calculated from the last plane of the lens in the direction of the propagation of radiation. The plano-convex refractive lenses have been mounted with the flat surface facing the detector. In this way, the meas-

ured distances can be precisely related to the back focal lengths of the lenses. The measured focal distances (from the last plane of the lenses) are equal to 98 and 130 mm for the diffractive lenses with $f = 115$ and $f = 151.5$ mm, respectively. Analogically, the measured focal distances for the refractive lenses with $f = 115$ and $f = 151.5$ mm are equal to 96 and 122 mm, respectively. Distances were calculated on the basis of the maximal registered intensity and are defined with the 2 mm resolution. According to the manufacturer, the back focal lengths of the two reference refractive lenses are equal to 98.7 and 130.5 mm (at 500 GHz).

The results obtained for two additional diffractive lenses with lower f -numbers are shown in Fig. 6. In both cases, the focal spots have been observed. The measured focal lengths of $f = 72.2$ mm

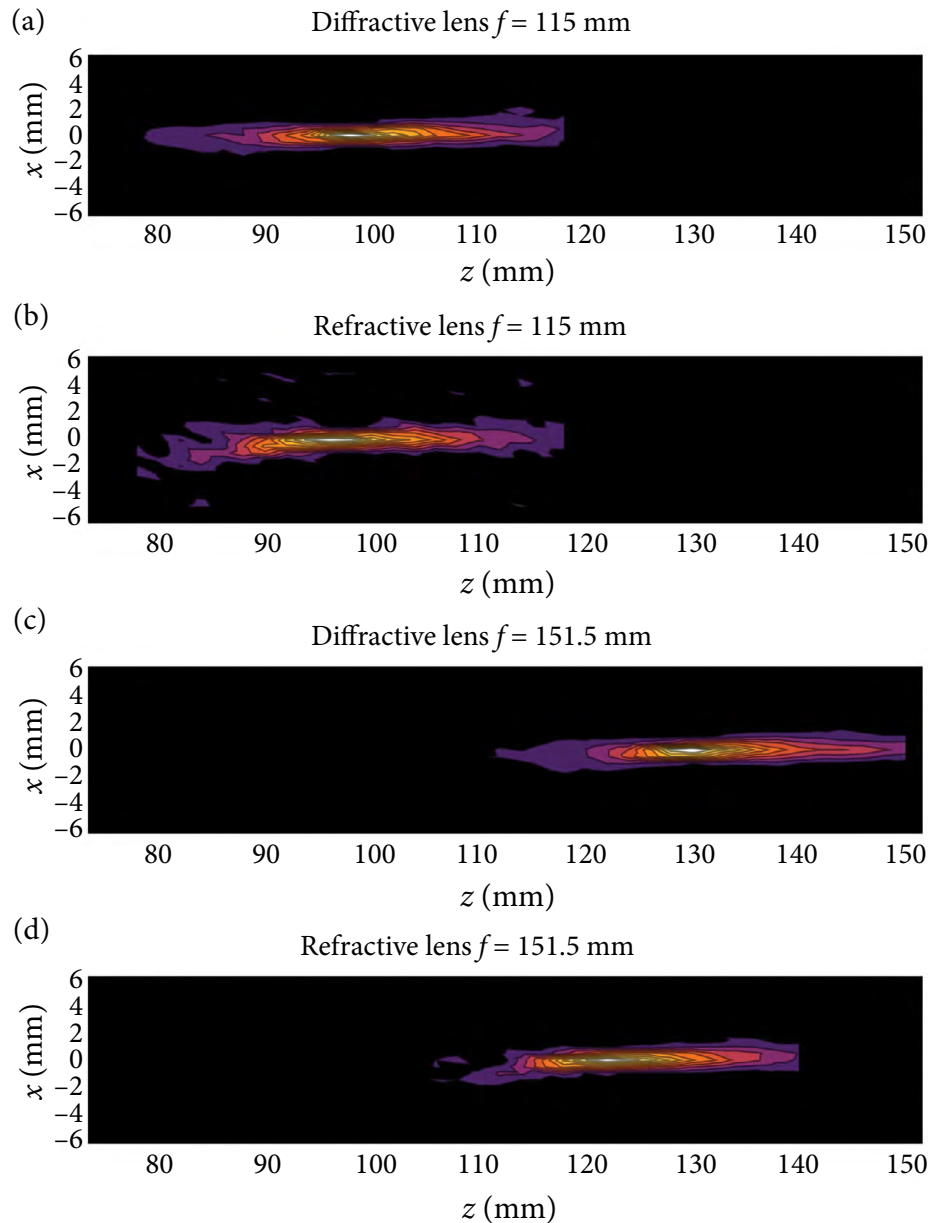


Fig. 5. The parallel (xz) scans in focal planes for (a) diffractive lens with $f = 115$ mm, (b) refractive lens with $f = 115$ mm, (c) diffractive lens with $f = 151.5$ mm and (d) refractive lens with $f = 151.5$ mm. The z distance is measured from the first plane of the lens.

and $f = 48.1$ mm lenses are equal to 61 and 40 mm. It can be observed that the registered intensity declines with the design focal length of the lenses. It is partially connected with the accuracy of the manufacturing. Lenses with shorter focal lengths have narrower zones, which are harder to accurately reproduce using FDM 3D printing. However, another mechanism limiting the registered power should also be named – the directivity of the detector. As investigated in Ref. [21], the directivity has a crucial impact on the measurements of

focal spots of low- f -number lenses. According to the manufacturer, the full 3 dB angular beamwidth of the antenna used for the detection is equal to 10° . This angle defines the cone of acceptance of the detector used. The diameter of a circular cross-section of this cone at the distances of 115, 72.2 and 48.1 mm is equal to 20.1, 12.6 and 8.4 mm, respectively. This means that only 7.0, 2.7 and 1.2% of the area of corresponding lenses are observed by the detector. In other words, it should be expected that the intensity registered for the $f = 72.2$ mm

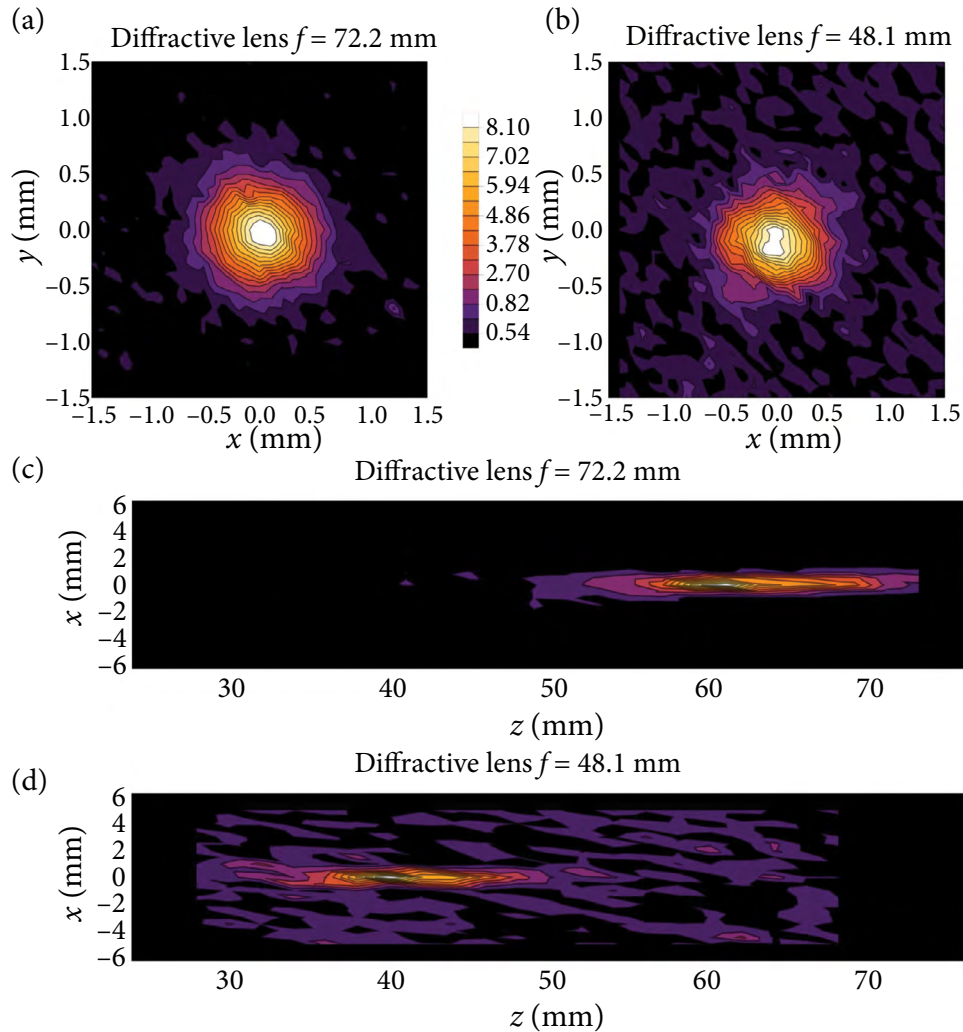


Fig. 6. The experimental scans obtained for two lenses with lower f-numbers: (a) xy scan for $f = 72.2$ mm lens, (b) xy scan for $f = 48.1$ mm lens, (c) xz scan for $f = 72.2$ mm lens and (d) xz scan for $f = 48.1$ mm lens.

and $f = 48.1$ mm lenses will correspond to 39 and 17% of the intensity registered for the $f = 115$ mm lens, respectively. In fact, the maximum intensities observed for these three lenses are equal to 16.49, 8.80 and 4.35, which translates to the relative attenuation of 53 and 26%. Therefore, the decline in the registered power is foremost caused by the measurement procedure. Taking this effect out of the equation, it can be found that the intensities measured for the $f = 72.2$ and $f = 48.1$ mm lenses constitute 73.6 and 65.3% of the intensity observed for the $f = 115$ mm lens. These values describe the actual diffraction efficiency of the manufactured low f-number lenses (with respect to the diffraction efficiency of the $f = 115$ mm lens).

The focal distances measured for all diffractive lenses are smaller than the theoretical ones

by a factor of $15.8 \pm 1\%$. It is connected with the illuminating wavefront, which is slightly convergent. This is an expected behaviour and does not influence the comparison between reference refractive lenses and designed diffractive lenses. The focal lengths measured for the reference lenses are also shorter than those of the catalog, in this case only by a factor of a few percent. This effect also comes from the convergence of the illuminating wave, which competes with the effect of the dispersion of the material used for manufacturing of the diffractive lenses.

4. Conclusions

Four diffractive lenses designed for 1 THz frequency have been fabricated from a COC filament

using FDM 3D printing. The additive manufacturing required the application of small, appropriately coated nozzles, a precisely calibrated printer, and multiple attempts at optimization of the printing parameters. Ultimately, the possibility of manufacturing DOEs for frequencies as high as 1 THz with this method has been demonstrated. To the best of the authors' knowledge, this is the highest operating frequency of a DOE manufactured using FDM 3D printing.

The described lenses work in accordance with the theoretical predictions. Moreover, in the direct comparison, lenses with longer focal lengths delivered more than double the optical power to the focal spots as their refractive counterparts, while preserving the same shape and dimensions of the focal spots. Furthermore, the applicability of the proposed method has been evaluated for lenses with relatively small f-numbers (0.95 and 0.63, respectively). Manufacturing of such lenses is challenging because of the fast-changing phase profile in the outer regions of the structure. In the refractive approach, it results in extremely thick and practically infeasible lenses, whereas in the diffractive approach, the outer zones of the lenses become very narrow. It is important to note that both lenses with the f-numbers of 0.95 and 0.63 were successfully manufactured and examined within the experimental setup. The results obtained are satisfactory and consistent with theoretical predictions.

References

- [1] F. Sizov, Brief history of THz and IR technologies, *Semicond. Phys. Quantum Electron. Optoelectron.* **22**(1), 67–79 (2019).
- [2] G.P. Gallerano and S. Biedron, in: *Proceedings of the 2004 FEL Conference* (2004) pp. 216–221.
- [3] F. Sizov, Terahertz radiation detectors: the state-of-the-art, *Semicond. Sci. Technol.* **33**(12), 123001 (2018).
- [4] I. Mehdi, J. Siles, C.P. Chen, and J.M. Jornet, in: *Proceedings of the 2018 Asia-Pacific Microwave Conference (APMC)* (IEEE, 2018) pp. 76–78.
- [5] V. Pavelyev, K. Tukmakov, Y.Y. Choporova, N. Osintseva, and B. Knyazev, Towards multi-channel terahertz telecommunication based on mode division multiplexing, *AIP Conf. Proc.* **2299**, 030002 (2020).
- [6] C. Castro, R. Elschner, T. Merkle, C. Schubert, and R. Freund, in: *Proceedings of the 2020 Third International Workshop on Mobile Terahertz Systems (IWMTS)* (IEEE, 2020) pp. 1–4.
- [7] E. Pickwell and V. Wallace, Biomedical applications of terahertz technology, *J. Phys. D* **39**(17), R301 (2006).
- [8] T. Amini, F. Jahangiri, Z. Ameri, and M.A. Hemmatian, A review of feasible applications of THz waves in medical diagnostics and treatments, *J. Lasers Med. Sci.* **12**, e92 (2021).
- [9] Z. Yan, L.-G. Zhu, K. Meng, W. Huang, and Q. Shi, THz medical imaging: from *in vitro* to *in vivo*, *Trends Biotechnol.* **40**(7), 816–830 (2022).
- [10] M. Naftaly and R.E. Miles, Terahertz time-domain spectroscopy for material characterization, *Proc. IEEE* **95**(8), 1658–1665 (2007).
- [11] A.G. Davies, A.D. Burnett, W. Fan, E.H. Linfield, and J.E. Cunningham, Terahertz spectroscopy of explosives and drugs, *Mater. Today* **11**(3), 18–26 (2008).
- [12] J.A. Spies, J. Neu, U.T. Tayvah, M.D. Capobianco, B. Pattengale, S. Ostresh, and C.A. Schmuttenmaer, Terahertz spectroscopy of emerging materials, *J. Phys. Chem. C* **124**(41), 22335–22346 (2020).
- [13] J.F. Federici, B. Schulkin, F. Huang, D. Gary, R. Barat, F. Oliveira, and D. Zimdars, THz imaging and sensing for security applications – explosives, weapons and drugs, *Semicond. Sci. Technol.* **20**(7), S266 (2005).
- [14] M.O. AlNabooda, R.M. Shubair, N.R. Rishani, and G. Aldabbagh, in: *2017 Sensors Networks Smart and Emerging Technologies (SENSET)* (IEEE, 2017) pp. 1–4.
- [15] G. Tzydynzhapov, P. Gusikhin, V. Muravev, A. Dremin, Y. Nefyodov, and I. Kukushkin, New real-time sub-terahertz security body scanner, *J. Infrared Millim. Terahertz Waves* **41**, 632–641 (2020).
- [16] S.F. Busch, M. Weidenbach, J.C. Balzer, and M. Koch, THz optics 3D printed with TOPAS, *J. Infrared Millim. Terahertz Waves* **37**, 303–307 (2016).

- [17] W.D. Furlan, V. Ferrando, J.A. Monsoriu, P. Zagrajek, E. Czerwińska, and M. Szustakowski, 3D printed diffractive terahertz lenses, *Opt. Lett.* **41**(8), 1748–1751 (2016).
- [18] A. Siemion, Terahertz diffractive optics – smart control over radiation, *J. Infrared Millim. Terahertz Waves* **40**(5), 477–499 (2019).
- [19] A. Siemion, A. Melaniuk, P. Zagrajek, P. Komorowski, M. Walczakowski, M. Surma, P. Sobotka, I. Ducin, and E. Czerwińska, in: *Proceedings of the 2020 23rd International Microwave and Radar Conference (MIKON)* (IEEE, 2020) pp. 225–228.
- [20] M. Kaluza, M. Surma, P. Komorowski, M. Walczakowski, and A. Siemion, in: *Proceedings of the 2022 47th International Conference on Infrared, Millimeter and Terahertz Waves (IRMMW-THz)* (IEEE, 2022) pp. 1–2.
- [21] P. Komorowski, A. Siemion, M. Walczakowski, and P. Zagrajek, The role of the directivity of various THz detectors in multiplexing systems, *Appl. Sci.* **12**(7), 3545 (2022).

3D SPAUSDINTI DIFRAKČINIAI LĖŠIAI 1 THz DAŽNIUI

P. Komorowski ^a, M. Kaluza ^b, M. Surma ^b, A. Siemion ^b

^a *Karo technologijos universiteto Optoelektronikos institutas, Varšuva, Lenkija*

^b *Varšuvos technologijos universiteto Fizikos fakultetas, Varšuva, Lenkija*

Special dedication to prof. Gintaras Valušis

In this special issue, I would like to thank you of being a person you are. I would like to wish you to continue what you are doing now with the same energy and smile. It is really outstanding and wonderful. Let me wish you always good health so that you can enjoy both scientific career and family life. I wish you to have time for yourself and to be happy from all that you have.

Prof. Dr. Agnieszka Siemion
Warsaw University of Technology